Mode Spectrum and Temporal Soliton Formation in Optical Microresonators

T. Herr,[1] V. Brasch,[1] J. D. Jost,[1] I. Mirgorodskiy,[1,2] G. Lihachev,[2] M. L. Gorodetsky,[2,3] and T. J. Kippenberg[1,*]
[1]*Ecole Polytechnique Fédérale de Lausanne (EPFL), 1015 Lausanne, Switzerland*
[2]*Faculty of Physics, M. V. Lomonosov Moscow State University, Moscow 119991, Russia*
[3]*Russian Quantum Center, Skolkovo 143025, Russia*
(Received 7 November 2013; published 15 September 2014)

The formation of temporal dissipative solitons in optical microresonators enables compact, high-repetition rate sources of ultrashort pulses as well as low noise, broadband optical frequency combs with smooth spectral envelopes. Here we study the influence of the microresonator mode spectrum on temporal soliton formation in a crystalline MgF_2 microresonator. While an overall anomalous group velocity dispersion is required, it is found that higher order dispersion can be tolerated as long as it does not dominate the resonator's mode structure. Avoided mode crossings induced by linear mode coupling in the resonator mode spectrum are found to prevent soliton formation when affecting resonator modes close to the pump laser frequency. The experimental observations are in excellent agreement with numerical simulations based on the nonlinear coupled mode equations. The presented results provide for the first time design criteria for the generation of temporal solitons in optical microresonators.

DOI: 10.1103/PhysRevLett.113.123901 PACS numbers: 42.65.Ky, 42.55.Sa, 42.62.Eh, 42.65.Tg

Optical temporal dissipative cavity solitons [1–3] can be formed and stably circulate in Kerr-nonlinear resonators (such as optical fiber cavities) with anomalous group velocity dispersion (GVD) that are driven by a monochromatic continuous wave pump laser [4]. Recently, these solitons have been discovered in crystalline MgF_2 microresonators where they allow for the generation of high-repetition rate ultrashort optical pulses and frequency comb spectra with a smooth sech^2-shaped spectral envelope associated with single cavity solitons [5]. The temporal width of the solitons is determined by the resonator dispersion and nonlinearity as well as the pump power and pump laser detuning [5,6]. The free spectral range (FSR) of the resonator, typically 10–100 GHz, determines the pulse repetition rate. Soliton formation is related to four-wave mixing based frequency comb generation in microresonators [7–16], where low and high noise operating regimes [13,17,18] have been identified. Here, techniques such as δ-Δ matching [18], self-injection locking [19,20], or parametric seeding [21] can be used to achieve a low noise operation. In contrast to these four-wave mixing based combs, the transition to the soliton regime [18] offers a unique combination of features, such as intrinsic low noise performance, direct pulse generation in the microresonator [5,22,23], and the smooth spectral envelope as shown in Fig. 1. These properties are critical to applications in, e.g., telecommunications [24–26], low phase noise microwave generation [19,27], precision spectroscopy, and frequency metrology [28,29].

Temporal dissipative cavity solitons in microresonators rely on the balance between Kerr nonlinearity and anomalous GVD in the presence of a monochromatic pump laser and loss. Theory predicts that soliton formation is possible in any Kerr-nonlinear microresonator with anomalous GVD [4,5,30–33]. While high effective nonlinearity and efficient nonlinear frequency conversion is routinely achieved in a wide variety of microresonator materials and geometries [7–16], soliton formation in optical microresonators has so far only been demonstrated in MgF_2

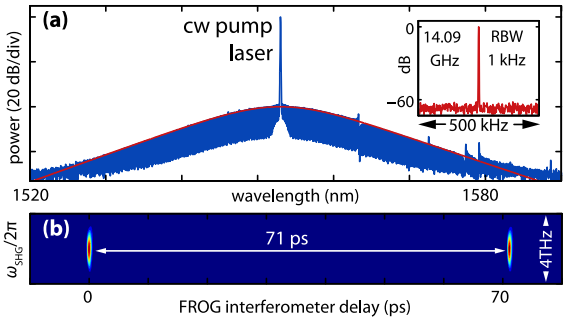

FIG. 1 (color online). (a) Measured optical spectrum with smooth sech^2-shaped spectral envelope (red line) of a single temporal soliton generated in a continuous wave laser driven crystalline high-finesse MgF_2 microresonator. The spectral 3-dB width of 13 nm (1.62 THz) corresponds to a soliton pulse duration of 194 fs (full width at half maximum). The pump power is 30 mW at a wavelength of 1552 nm. The inset shows the resolution bandwidth (RBW) limited rf signal at a frequency of 14.09 GHz corresponding to the soliton pulse repetition rate. (b) Frequency resolved optical gating (FROG) of the ultrashort pulses outcoupled from the resonator. The pulses are separated by 71 ps corresponding to the inverse repetition rate (The FROG measurement uses second harmonic generation in a beta barium borate crystal. The second harmonic frequency $\omega_{\mathrm{SHG}}/2\pi$ is centered around 384 THz. After attenuation of the pump laser, the remaining soliton spectrum has been amplified to approximately 30 mW of the average optical power. Conventional fiber is used for dispersion compensation.

microresonators [5] where the characteristic spectral sech^2-shaped envelope and stable ultrashort pulses have been observed [cf. Fig. 1(a)].

Here, it is revealed for the first time that the mode structure of the microresonator is the decisive requirement for the generation of solitons.

The mode structure of an optical microresonator typically deviates from an anomalous GVD and is affected by higher order dispersion and linear coupling (e.g., via scattering) between multiple optical mode families [34–37]. While a microresonator has typically multiple mode families [cf. Fig. 2(a)] [38–40], the soliton is always supported by only a single mode family at a time. The latter follows from the energy and momentum conservation in the nonlinear parametric frequency conversion processes [7]. However, the mode frequencies of the soliton supporting mode family may be shifted due to the presence of the other mode families. This is different from temporal dissipative optical solitons in single mode fiber loop resonators [4] where interactions between mode families do not normally occur. Understanding temporal dissipative solitons in a mode family that deviates from a purely anomalous GVD is essential to achieve soliton formation in other microresonator platforms such as CMOS compatible chip-based microresonators [11,12].

The dispersion (i.e., the mode structure) of a microresonator can be described in terms of its resonance frequencies ω_μ using the parameters D_1, D_2, D_3, etc., which correspond to the FSR in rad/s, the second order dispersion and higher order dispersion parameters, respectively, [18,41]

$$\omega_\mu = \omega_0 + D_1\mu + \frac{1}{2}D_2\mu^2 + \frac{1}{6}D_3\mu^3 + \cdots. \quad (1)$$

Here, μ denotes the relative mode number with respect to the pump (designated by $\mu = 0$). The parameters D_2 and D_3 are related to the GVD parameters β_2 and β_3 via

$$D_2 = -\frac{c}{n}D_1^2\beta_2. \quad (2)$$

$$D_3 = -\frac{c}{n}D_1^3\beta_3 + 3\frac{c^2}{n^2}D_1^3\beta_2^2 \approx -\frac{c}{n}D_1^3\beta_3.$$

A positive D_2 corresponds to an anomalous GVD leading to a parabolic deviation of the resonance frequencies from an equidistant D_1-spaced frequency grid [cf. the grey curve in Figs. 2(c) and 2(d)]. This anomalous GVD can be modified by higher order terms such as D_3 as illustrated schematically in Fig. 2(c). The dispersion coefficients D_2, D_3, etc. can be estimated analytically [38,40,42–44] or numerically [35,45–47] by taking material and geometrical dispersive effects into account. The coupling between mode families can additionally modify the mode frequencies [34–37] and lead to avoided crossings as illustrated schematically in Fig. 2(d). To investigate the dispersion requirements for soliton formation in an experimental system, broadband frequency comb assisted scanning laser spectroscopy [35] is used to precisely measure the complex mode structure of a MgF_2 microresonator (FSR 14.09 GHz)

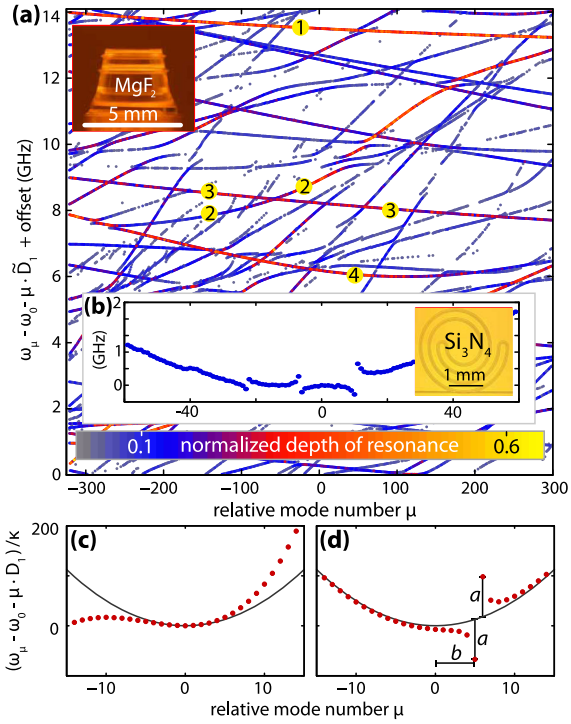

FIG. 2 (color online). (a) Mode structure of a MgF_2 resonator with linewidths in the range of 50–500 kHz and an approximate FSR of 14.09 GHz, as measured by frequency comb assisted diode laser spectroscopy [35]. Dots forming a continuous line represent a particular mode family. Different free spectral ranges correspond to different slopes of the lines, whereas dispersion and variation of the free spectral range show as a curvature of the lines (convex and concave curvatures correspond to anomalous and normal GVD, respectively). The dispersion can be strongly affected by mode crossings. Four specific mode families have been numbered by yellow labels. The color codes the measured resonance depth and helps to track particular mode families. (b) Comparable measurement of the fundamental TM11 mode in a Si_3N_4 microresonator with a resonator linewidth of 350 MHz and approximate FSR of 76 GHz (consisting of a 800 nm high and 2 μm wide Si_3N_4 waveguide embedded in SiO_2). The mode family shows signs of mode coupling to other mode families. (c) Illustration of higher order dispersion with $D_3 > 0$. The gray line indicates anomalous GVD described by D_2 only. (d) Illustration of mode coupling induced mode frequency shift altering the dispersion properties locally. A simple parametrization using magnitude a and position b of the avoided mode crossing can be used for numerical modeling.

[16,48,49] over a spectral span exceeding 8 THz (including tens of mode families). The measured mode structure is visualized in Fig. 2(a). Here, for each detected mode family and relative mode number μ, the mode frequency is given with respect to a common equidistant frequency grid with a spacing of $\tilde{D}_1/2\pi = 14.095$ GHz (close to the approximate average FSR, but chosen arbitrarily). Mode families with different FSRs that cross other mode families or that show modified dispersion due to avoided mode crossings can be observed. Some mode families exhibit normal GVD; other mode families exhibit anomalous GVD. The inset in

Fig. 2(a) shows that the effects of interacting modes are not only present in the case of a crystalline MgF_2 microresonator but also occur in a Si_3N_4 microresonator that, due to its small cross section, supports only few mode families.

Next, the dispersion of four individual mode families is related to their potential of supporting temporal solitons. All four mode families allow for efficient nonlinear frequency conversion. The latter is verified by detecting the parametrically frequency converted laser light (i.e., the outcoupled optical comb spectrum with the pump wavelength filtered out, using a narrow-band fiber-Bragg grating) with a photo detector. The converted light signal also provides a direct means of detecting soliton formation. The latter exploits the fact that the formation of solitons coincides with discrete steps in the converted light signal [cf. Figs. 3(a) and 3(d), right column] that are observed when the pump laser is scanned over the resonance (cf. see the Supplemental Material [50] as well as the Supplemental Material of Ref. [5]). The signals of the converted laser light for the four pumped modes are shown in Fig. 3 (right column) as a function of the scan time. Despite significant nonlinear frequency conversion in all four mode families, only two mode families (1 and 4) exhibit soliton formation. To understand why, the dispersion properties of all four modes are investigated based on the data shown in Fig. 2(a). Figure 3 (left column) shows the deviation of the resonance frequencies of the individual mode families from an equidistant frequency grid defined by the FSR (i.e., $D_1/2\pi$) of the mode family at the pumped resonance $\mu = 0$. A perfectly anomalous GVD, i.e., $D_2 > 0$ and vanishing higher order dispersion terms correspond to a convex parabolic curve. This case is closely realized for mode family 1 ($D_2/2\pi = 1.9$ kHz, $D_3/2\pi \approx 0$), which also shows the characteristic step signature [5] of soliton formation [Fig. 3(a), right]. Mode family 2 [Fig. 3(b)] is not characterized by an anomalous GVD and does not show signs of soliton formation. Mode family 3 [Fig. 3(c)] exhibits an overall anomalous GVD that is, however, disturbed locally by two avoided mode crossings in the spectral proximity of the pumped mode. The mode family does not support solitons. In contrast, solitons are generated in mode family 4 [Fig. 3(d)], which in addition to a dominating anomalous GVD ($D_2/2\pi = 21$ kHz) exhibits a noticeable higher order contribution ($D_3/2\pi = 90$ Hz). Moreover, the smooth dispersion curve is disturbed by two avoided mode crossings well separated in terms of mode number from the pumped mode. These measurements suggest that the formation of the soliton is robust against a certain contribution of higher order dispersion as well as a local mode frequency shift induced by mode coupling. However, an overall GVD that is not generally anomalous (as in the case of mode family 2) or avoided mode crossings too close to the pumped mode (as in the case of mode family 3) appears to prevent soliton formation.

In the following, to test these experimentally motivated hypotheses, we utilize numerical simulations based on

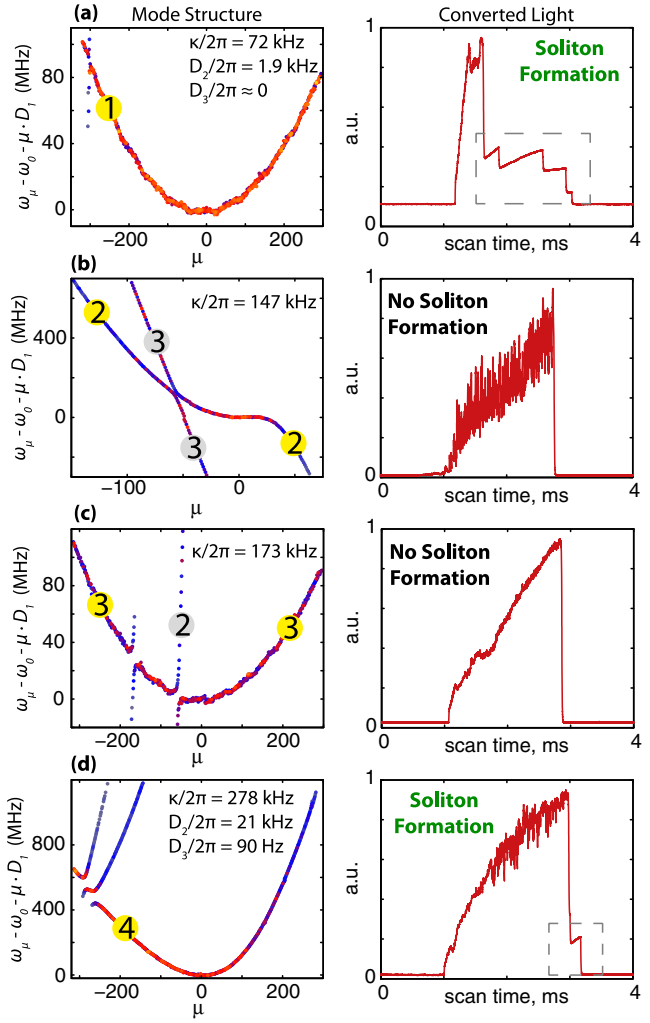

FIG. 3 (color online). Experimental investigation of soliton formation in different dispersion scenarios in a MgF_2 microresonator. (a) and (d) Soliton formation is observed in resonance families 1 and 4 of Fig. 1, which show an almost ideal $D_2 > 0$ dominated anomalous GVD. The soliton formation is detected by the observation of the step signature in the converted light signal (inside the dashed grey box). (b) and (c) Soliton formation is not observed in mode families 2 and 3 where strong deviations from D_2 dominated dispersion are present. The coupled pump power is $\mathcal{O}(1\text{mW})$ at a wavelength of 1552 nm.

the nonlinear coupled mode equations (cf. Supplemental Material [50] and the Supplemental Material of Ref. [5]) [32,51,52]. A key advantage of this numerical method is that it allows for the definition and simulation of arbitrary and complex mode structures ω_μ. To investigate whether a particular mode structure allows for soliton formation, pump laser scans that can lead to the formation of solitons [5] are numerically simulated. To ensure deterministic computational evolution into a single soliton state, the unperturbed analytical single soliton waveform [5] is used for seeding the simulation (cf. Supplemental Material [50]). For each simulated pump laser scan the maximum ratio of peak to average power inside the microresonator is computed. This ratio serves as a reliable indicator of soliton

formation inside the microresonator. By propagating the simulation over a time scale much longer than the dynamic time scale of the cavity it is verified that the generated solitons are stable. Throughout the simulation, typical microresonator parameters of $\kappa/2\pi = 1$ MHz, a FSR of 35 GHz, an effective nonlinearity of $\gamma = 4 \times 10^{-4}$ m^{-1} W^{-1}, and a pump power of 100 mW at 1.55 μm wavelength are assumed. The simulations only include generic microresonator properties and are thus platform independent (cf. Supplemental Material [50]) [5].

First, to study the effect of higher order dispersion, the optical modes are defined according to Eq. (1) with varying D_2 and D_3 (the offset ω_0 and the linear term D_1 can be chosen arbitrarily). The numerical results in Figs. 4(a), 4(b), and 4(c) show that nonzero values of D_3 require a minimal magnitude of the coefficient D_2 to allow for soliton formation. The maximum soliton peak intensities and shortest soliton pulse durations are achieved for vanishing D_3 and small values of $D_2 > 0$. Figure 4(a) is a contour plot of the peak intracavity intensities as a function of D_2 and D_3. The peak intensities are invariant under a change of sign in D_3. Higher order dispersion leads to soliton induced dispersive wave emission [31,33,53] (also known as soliton Cherenkov radiation [54]).

Second, the effect of avoided mode crossings is studied in a simplified two-parameter model. Here the mode frequencies are defined according to

$$\omega_\mu = \omega_0 + D_1\mu + \frac{1}{2}D_2\mu^2 + \frac{a/2}{\mu - b - 0.5} \tag{3}$$

to phenomenologically mimic the effect of resonance frequency shifts induced by an avoided mode crossing. The parameters a and b specify the magnitude of this frequency shift and the frequency separation of the avoided crossing from the pumped mode [cf. Fig. 2(d)]. The maximum resonance frequency shift of a occurs for the modes with mode numbers $\mu = b$ and $\mu = b + 1$. In the Supplemental Material it is shown that this two-parameter model can be used to simulate the effect of mode coupling without the necessity of including another mode family into the coupled mode equations [50]. The results of the simulations for various values of a and b are shown in Figs. 4(d), 4(e), and 4(f). Here, Fig. 4(d) shows the peak power as a function of the strength and location of the mode crossing. The contour plot exhibits a point symmetry, reflecting the equivalence of the mode shifts defined by $\{+a, +b\}$ and $\{-a, -b\}$, respectively. While Fig. 4(d)

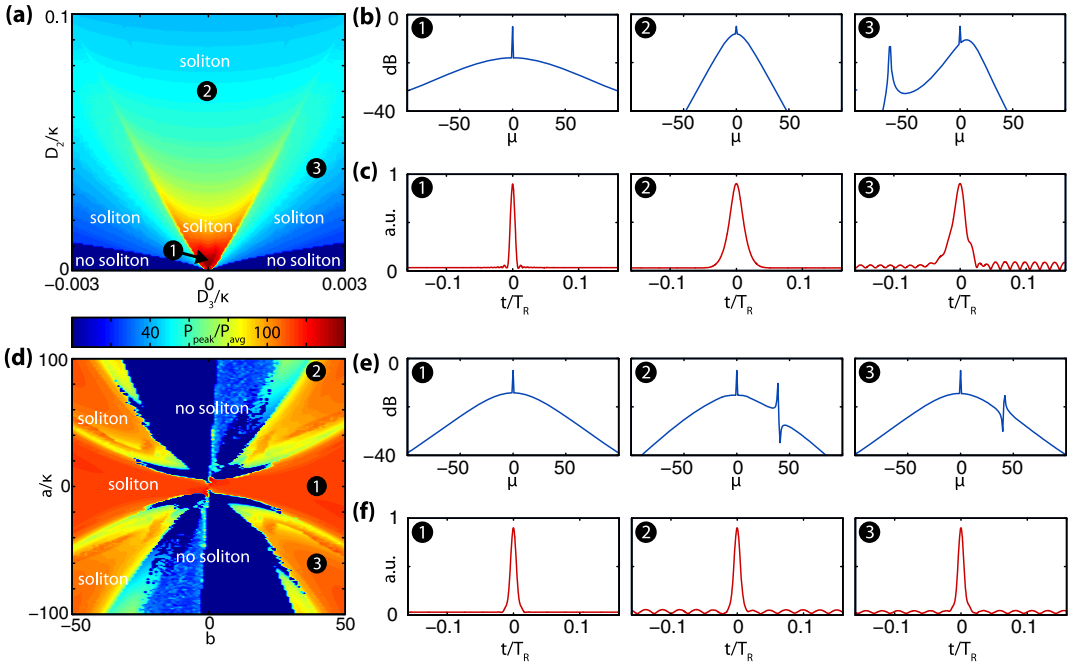

FIG. 4 (color online). Numerical investigation of soliton formation in different dispersion scenarios. (a) The ratio $P_{\mathrm{peak}}/P_{\mathrm{avg}}$ of peak to average intracavity power is used as an indicator of soliton formation (which results in high peak power) for different combinations of D_2 and D_3. (b) Optical spectra for different parameters simulated in panel (a) (1, 2, 3) show a narrow spectral width for high values of D_2 and asymmetric spectra, as well as dispersive wave phenomena (peak at $\mu = -65$) for nonzero D_3. (c) Temporal field envelope inside the microresonator corresponding to the spectra shown in panel (b). The soliton pulse duration lengthens for larger values of D_2. Oscillatory features in the background field appear for nonzero D_3. (d) The high ratio of peak to average power is used as an indicator of soliton formation for different situations characterized by an avoided mode crossing that is parametrized by magnitude a and distance b from the pump laser [cf. Fig. 2(d)]. (e) Optical spectra for different simulation parameters in panel (d) (1, 2, 3) show the characteristic "up-down" feature induced by an avoided mode crossing. (f) Temporal field envelope inside the microresonator corresponding to panel (e). The pulses have the same duration but oscillatory features in the background field appear in the presence of avoided mode crossings.

reveals a rich and complex structure, it shows that the larger the spectral separation b of the mode crossing from the pumped mode ($\mu = 0$), the higher the magnitude a of the mode crossing can be without preventing soliton formation. The presence of mode crossing manifests itself in the optical spectrum as characteristic features, where the spectral intensities are increased on one side of the avoided crossing and decreased on the other [cf. Fig. 4(e), trace 2 and 3] [37]. These features are evidenced experimentally in Fig. 1(a). Increasing the magnitude of the mode crossing a to larger values eventually inhibits the formation of solitons.

In summary, we have shown experimentally and numerically that a D_2 dominated anomalous GVD as well as the absence of strong mode crossings close to the pump frequency are essential prerequisites for the generation of temporal dissipative solitons in optical microresonators. A low number of avoided mode crossings can be achieved by reducing mode coupling and by designing single mode resonators. These platform independent findings provide, for the first time, generic design criteria for microresonator based ultrashort pulse generators.

This work was supported by the Swiss National Science Foundation (T. H.), the European Space Agency (V. B), a Marie Curie IIF (J. D. J), the Eurostars program, the DARPA QuASAR program, and RFBR Grant No. 13-02-00271 (M. L. G), as well as by the Space Optical Clock program (FP7, Grant Agreement No. 263500).

*tobias.kippenberg@epfl.ch

[1] L. A. Lugiato and R. Lefever, Phys. Rev. Lett. **58**, 2209 (1987).
[2] S. Wabnitz, Opt. Lett. **18**, 601 (1993).
[3] N. Akhmediev and A. Ankiewicz, *Dissipative Solitons: From Optics to Biology and Medicine* (Springer, Berlin, 2008).
[4] F. Leo, S. Coen, P. Kockaert, S.-P. P. Gorza, P. Emplit, and M. Haelterman, Nat. Photonics **4**, 471 (2010).
[5] T. Herr, V. Brasch, J. D. Jost, C. Y. Wang, N. M. Kondratiev, M. L. Gorodetsky, and T. J. Kippenberg, Nat. Photonics **8**, 145 (2014).
[6] S. Coen and M. Erkintalo, Opt. Lett. **38**, 1790 (2013).
[7] P. Del'Haye, A. Schliesser, O. Arcizet, T. Wilken, R. Holzwarth, and T. Kippenberg, Nature (London) **450**, 1214 (2007).
[8] A. A. Savchenkov, A. B. Matsko, V. S. Ilchenko, I. Solomatine, D. Seidel, and L. Maleki, Phys. Rev. Lett. **101**, 093902 (2008).
[9] I. S. Grudinin, N. Yu, and L. Maleki, Opt. Lett. **34**, 878 (2009).
[10] L. Razzari, D. Duchesne, M. Ferrera, R. Morandotti, S. Chu, B. E. Little, and D. J. Moss, Nat. Photonics **4**, 41 (2010).
[11] J. S. Levy, A. Gondarenko, M. A. Foster, A. C. Turner-Foster, A. L. Gaeta, and M. Lipson, Nat. Photonics **4**, 37 (2010).
[12] M. A. Foster, J. S. Levy, O. Kuzucu, K. Saha, M. Lipson, and A. L. Gaeta, Opt. Express **19**, 14233 (2011).
[13] S. B. Papp and S. A. Diddams, Phys. Rev. A **84**, 053833 (2011).
[14] T. J. Kippenberg, R. Holzwarth, and S. A. Diddams, Science **332**, 555 (2011).
[15] W. Liang, A. A. Savchenkov, A. B. Matsko, V. S. Ilchenko, D. Seidel, and L. Maleki, Opt. Lett. **36**, 2290 (2011).
[16] C. Wang, T. Herr, P. Del'Haye, A. Schliesser, J. Hofer, R. Holzwarth, T. Hänsch, N. Picqué, and T. Kippenberg, Nat. Commun. **4**, 1345 (2013).
[17] F. Ferdous, H. Miao, D. E. Leaird, K. Srinivasan, J. Wang, L. Chen, L. T. Varghese, and A. M. Weiner, Nat. Photonics **5**, 770 (2011).
[18] T. Herr, K. Hartinger, J. Riemensberger, C. Y. Wang, E. Gavartin, R. Holzwarth, M. L. Gorodetsky, and T. J. Kippenberg, Nat. Photonics **6**, 480 (2012).
[19] J. Li, H. Lee, T. Chen, and K. J. Vahala, Phys. Rev. Lett. **109**, 233901 (2012).
[20] P. D. Haye, S. B. Papp, and S. A. Diddams, Phys. Rev. Lett. **112**, 043905 (2014).
[21] S. B. Papp, P. D. Haye, and S. A. Diddams, Opt. Express **21**, 17615 (2013).
[22] M. Peccianti, A. Pasquazi, Y. Park, B. E. Little, S. T. Chu, D. J. Moss, and R. Morandotti, Nat. Commun. **3**, 765 (2012).
[23] K. Saha, Y. Okawachi, B. Shim, J. S. Levy, M. A. Foster, R. Salem, A. R. Johnson, M. R. E. Lamont, M. Lipson, and A. L. Gaeta, Opt. Express **21**, 1335 (2013).
[24] J. S. Levy, K. Saha, Y. Okawachi, M. a. Foster, A. L. Gaeta, and M. Lipson, IEEE Photonics Technol. Lett. **24**, 1375 (2012).
[25] P.-H. Wang, F. Ferdous, H. Miao, J. Wang, D. E. Leaird, K. Srinivasan, L. Chen, V. Aksyuk, and A. M. Weiner, Opt. Express **20**, 29284 (2012).
[26] J. Pfeifle, M. Lauermann, D. Wegner, V. Brasch, T. Herr, K. Hartinger, J. Li, D. Hillerkuss, R. Schmogrow, R. Holzwarth *et al.*, Nat. Photonics **8**, 375 (2014).
[27] A. A. Savchenkov, A. B. Matsko, D. Strekalov, M. Mohageg, V. S. Ilchenko, and L. Maleki, Phys. Rev. Lett. **93**, 243905 (2004).
[28] T. Udem, R. Holzwarth, and T. W. Hänsch, Nature (London) **416**, 233 (2002).
[29] S. T. Cundiff and J. Ye, Rev. Mod. Phys. **75**, 325 (2003).
[30] A. B. Matsko, A. A. Savchenko, W. Liang, V. S. Ilchenkko, D. Sediel, and L. Maleki, Opt. Lett. **36**, 2845 (2011).
[31] S. Coen, H. G. Randle, T. Sylvestre, and M. Erkintalo, Opt. Lett. **38**, 37 (2013).
[32] Y. K. Chembo and C. R. Menyuk, Phys. Rev. A **87**, 053852 (2013).
[33] M. R. E. Lamont, Y. Okawachi, and A. L. Gaeta, Opt. Lett. **38**, 3478 (2013).
[34] T. Carmon, H. G. L. Schwefel, L. Yang, M. Oxborrow, A. D. Stone, and K. J. Vahala, Phys. Rev. Lett. **100**, 103905 (2008).
[35] P. Del'Haye, O. Arciezt, M. L. Gorodetsky, R. Holzwarth, and T. J. Kippenberg, Nat. Photonics **3**, 529 (2009).
[36] A. A. Savchenkov, A. B. Matsko, W. Liang, V. S. Ilchenko, D. Seidel, and L. Maleki, Opt. Express **20**, 27290 (2012).
[37] I. S. Grudinin, L. Baumgartel, and N. Yu, Opt. Express **21**, 26929 (2013).
[38] S. Schiller, Appl. Opt. **32**, 2181 (1993).
[39] E. A. J. Marcatili, Bell Syst. Tech. J. **48**, 2071 (1969).
[40] Y. A. Demchenko and M. L. Gorodetsky, J. Opt. Soc. Am. B **30**, 3056 (2013).

[41] A. A. Savchenkov, A. B. Matsko, W. Liang, V. S. Ilchenko, D. Seidel, and L. Maleki, Nat. Photonics **5**, 293 (2011).
[42] M. L. Gorodetsky and V. S. Ilchenko, Opt. Commun. **113**, 133 (1994).
[43] M. Gorodetsky and A. E. Fomin, IEEE J. Sel. Top. Quantum Electron. **12**, 33 (2006).
[44] M. L. Gorodetsky and A. E. Fomin, Quantum Electron. **37**, 167 (2007).
[45] M. Oxborrow, IEEE Trans. Microwave Theory Tech. **55**, 1209 (2007).
[46] J. Riemensberger, K. Hartinger, T. Herr, V. Brasch, R. Holzwarth, and T. J. Kippenberg, Opt. Express **20**, 27661 (2012).
[47] K. Saha, Y. Okawachi, J. S. Levy, R. K. W. Lau, K. Luke, M. A. Foster, M. Lipson, and A. L. Gaeta, Opt. Express **20**, 26935 (2012).
[48] W. Liang, V. S. Ilchenko, A. A. Savchenko, A. B. Matsko, D. Seidel, and L. Maleki, Opt. Lett. **35**, 2822 (2010).
[49] I. S. Grudinin, L. Baumgartel, and N. Yu, Opt. Express **20**, 6604 (2012).
[50] See the Supplemental Material at http://link.aps.org/supplemental/10.1103/PhysRevLett.113.123901 for details on the numerical simulations and experimental soliton generation.
[51] Y. K. K. Chembo and N. Yu, Phys. Rev. A **82**, 033801 (2010).
[52] T. Hansson, D. Modotto, and S. Wabnitz, Opt. Commun. **312**, 134 (2014).
[53] M. Erkintalo, Y. Q. Xu, S. G. Murdoch, J. M. Dudley, and G. Genty, Phys. Rev. Lett. **109**, 223904 (2012).
[54] N. Akhmediev and M. Karlsson, Phys. Rev. A **51**, 2602 (1995).